The Astrophysical Journal, 623:148–158, 2005 April 10

THE DISTANCE AND METALLICITY OF THE NEWLY DISCOVERED, NEARBY IRREGULAR GALAXY HIZSS 3[1]

David R. Silva
European Southern Observatory, Karl-Schwarzschild-Strasse 2,
Garching bei München, D-85748, Germany; dsilva@eso.org

Philip Massey
Lowell Observatory, 1400 West Mars Hill Road, Flagstaff, AZ 86001; phil.massey@lowell.edu

Kathleen DeGioia-Eastwood
Department of Physics and Astronomy, Northern Arizona University, P.O. Box 6010,
Flagstaff, AZ 86011-6010; kathy.eastwood@nau.edu

and

P. A. Henning
Institute for Astrophysics, University of New Mexico, 800 Yale Boulevard NE,
Albuquerque, NM 87131-1156; henning@as.unm.edu
Received 2004 September 3; accepted 2004 December 8

ABSTRACT

HIZSS 3 is an H I source in the Zone of Avoidance. Its radio characteristics are consistent with it being a previously unknown, nearby (∼1.8 Mpc), low-mass dwarf irregular (dIrr) galaxy. Optical observations have shown that it contains a modest H II region, but they failed to reveal a resolved stellar population. New spectroscopic observations of the H II region obtained at the MMT Observatory are presented here. They are used to derive the line-of-sight extinction [$E(B-V) = 1.41 \pm 0.04$] and gas metallicity ($\log \mathrm{O/H} + 12 \sim 7.8$) of the H II region. New near-IR imaging observations obtained at the ESO Very Large Telescope are also presented here. These images clearly reveal the resolved stellar population of HIZSS 3 for the first time. Narrowband Paβ images of the H II region are used in combination with previously published Hα data to obtain an independent line-of-sight extinction estimate: $E(B-V) = 1.32 \pm 0.04$. The adopted foreground extinction is $E(B-V) = 1.36 \pm 0.06$. Using the K-band luminosity function and K, $J-K$ color-magnitude diagram, the apparent magnitude and color of the tip of the red giant branch are derived. In turn, these parameters are combined with the adopted foreground extinction to estimate the distance (1.69 ± 0.07 Mpc) and mean red giant branch metallicity ([Fe/H] = −0.5 ± 0.1). As an ensemble, these new observations significantly strengthen the conclusion that HIZSS 3 is a newly discovered low-mass dIrr galaxy lurking behind the Milky Way in the outskirts of the Local Group.

Subject headings: galaxies: dwarf — galaxies: individual (HIZSS 3) — galaxies: irregular

Online material: color figures

1. INTRODUCTION

HIZSS 3 ($l = 217.7$, $b = 0.01$) is an H I source in the Zone of Avoidance (ZOA), i.e., the region near the Galactic plane in which foreground extinction from dust and gas causes an apparent decrease in the surface density of extragalactic objects at optical wavelengths. HIZSS 3 was originally detected at 21 cm by the Dwingeloo Obscured Galaxies Survey (Henning et al. 1998; Rivers et al. 1999; Rivers 2000) and the H I Parkes ZOA Shallow Survey (HIZSS; Henning et al. 2000). The name (HIZSS 3) comes from the list in the latter paper. Based on Very Large Array (VLA)[2] observations, it has an H I mass of $2 \times 10^7\ M_\odot$, assuming a distance of 1.8 Mpc estimated from the heliocentric velocity (280 km s^{-1}) of the H I source transformed to the Local Group velocity centroid and assuming no peculiar velocity (Massey et al. 2003, hereafter MHK03). Given the low radial velocity of the H I gas, this distance (and hence mass) estimate must be considered unreliable. A modest Hα source at the same heliocentric velocity and within the VLA 21 cm contours of HIZSS 3 was detected by MHK03. This star formation site is not spatially coincident with the main, resolved H I peak in the MHK03 VLA 21 cm map but rather with a semiresolved secondary peak. *BVRI* images obtained by MHK03 that were centered on the 21 cm peak failed to definitively detect any stars associated with HIZSS 3, likely because of a combination of poor seeing (∼3″) and high foreground extinction (estimated $A_B = 4.7$ mag; Henning et al. 2000).

As discussed by MHK03, the characteristics of HIZSS 3 suggest that it is a newly discovered, nearby dwarf (dIrr) irregular galaxy. At an estimated distance of 1.8 Mpc, HIZSS 3 lies beyond the zero-velocity boundary of the Local Group. However, this 21 cm redshift-based distance estimate relies on the assumption that HIZSS 3 has negligible peculiar velocity, which is true for most but not all (e.g., Leo I) Local Group members. Thus, Local Group membership cannot be ruled out on the basis of existing radio data.

[1] The optical spectroscopic observations reported here were obtained at the MMT Observatory, a joint facility of the Smithsonian Institution and the University of Arizona. The near-IR imaging observations reported here were collected at the European Southern Observatory, Cerro Paranal, Chile, within observing program 271.B-5047.

[2] The VLA is operated by the National Radio Astronomy Observatory, which is a facility of the National Science Foundation, operated under cooperative agreement by Associated Universities, Inc.

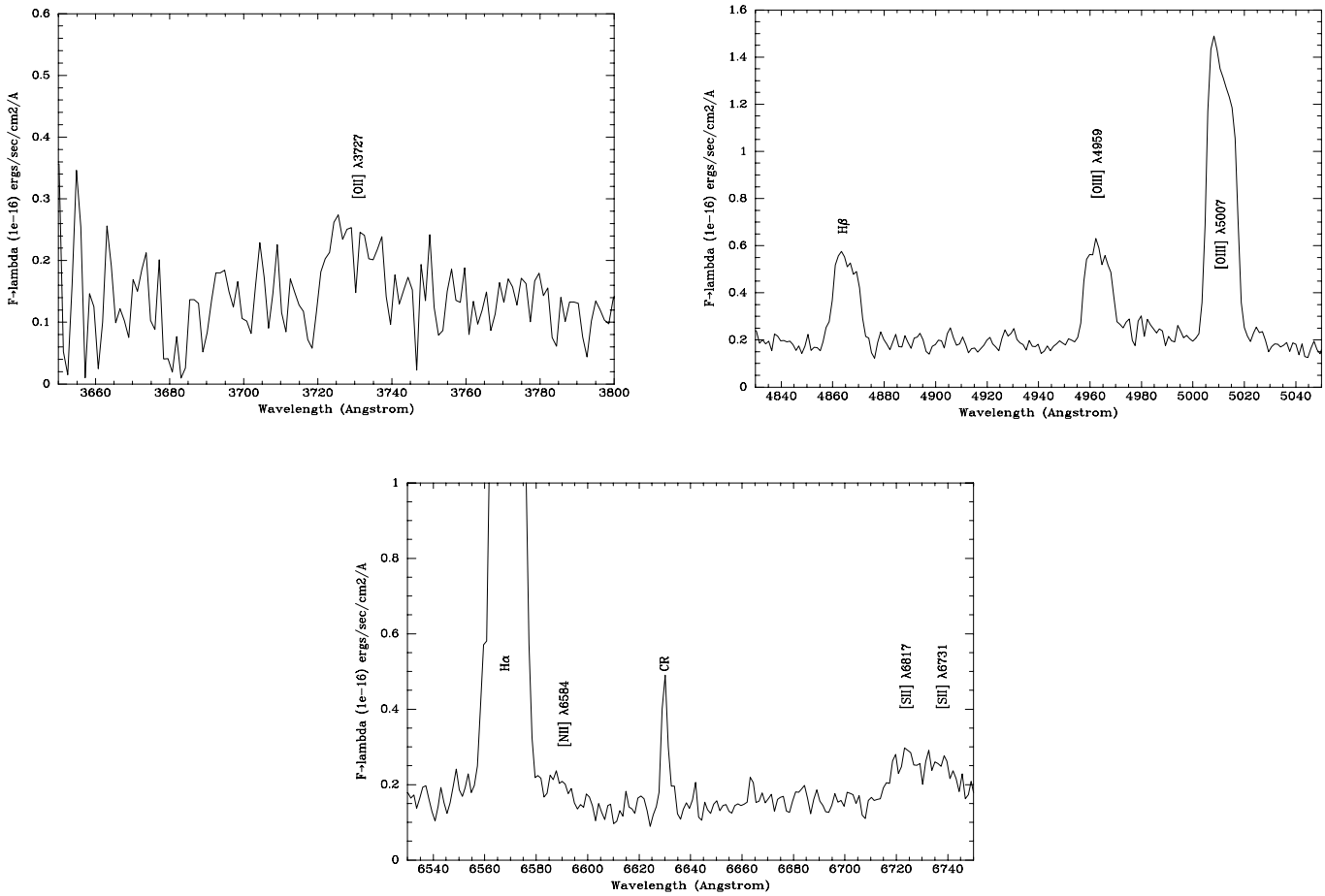

FIG. 1.—Three spectral regions in our summed spectrum of the H II region in HIZSS 3.

In this paper, new data are presented from the ESO Very Large Telescope (VLT) and MMT Observatory facilities. The MMT spectroscopic observations are used to measure foreground reddening and the nebular metallicity of the H II region detected by MHK03. Foreground reddening is independently estimated using VLT near-IR photometric observations and a different methodology. The two foreground reddening estimates are found to be essentially identical. More significantly, the stellar component of HIZSS 3 is directly observed for the first time in near-IR images obtained with the VLT. Using these images, near-IR luminosity functions, as well as a color-magnitude diagram (CMD) are constructed. In combination, these functions and the CMD are used to estimate the metallicity and distance of the tip of the red giant branch (TRGB). In agreement with MHK03, the new derived properties of HIZSS 3 presented here are consistent with a previously unknown dwarf irregular galaxy on the outskirts of the Local Group.

2. OBSERVATIONS AND DATA PROCESSING

2.1. *MMT Observations*

Optical spectroscopy of the H II region found in HIZSS 3 by MHK03 was obtained on 2003 November 21 UT at the 6.5 m MMT Observatory by P. M. and K. D. E. The primary goal of these observations was to determine foreground reddening from spectrophotometry of Hβ relative to Hα, with a secondary goal of determining the oxygen abundance if the [O II] λ3727 nebular line could be detected despite the high reddening. The data were obtained with the MMT Blue Channel spectrograph using a 500 lines mm^{-1} grating with a dispersion of 1.18 Å pixel^{-1} and a 2688×512 backside-processed CCD provided by the University of Arizona Imaging Technology Laboratory. In order to allow in more light, the slit was opened to 3$''$.5, resulting in a resolution of 10 pixels (12 Å). No blocking filter was used in order to maximize the throughput, a seemingly safe choice given that first-order Hα would be contaminated by second-order light at 3280 Å. While this proved to be a good choice for the H II region, the bluest flux standards (G191-B2B and Feige 34) showed evidence of a 10% contamination in the red compared to the flux standard, Hiltner 600, which has a large Balmer jump. Thus, only observations of the latter were used for the flux calibration. The HIZSS 3 observations were made as eight 1200 s integrations, with the slit of the spectrograph reset to the parallactic angle at the beginning of each integration.

IRAF[3] was used for all data processing. Examination of the two-dimensional spectra revealed that the spatial distribution of the nebular lines was localized to 1$''$–2$''$, coincident with the H II region. The spectra were extracted using the trace of an observation of the nearby offset star as the template. Sky background was determined from each side of the extraction aperture and subtracted. There is obvious structure within the slit due to brightness variations of the nebula, and this structure changed with the rotation angle. Therefore, the intensities of the strongest lines (Hα, Hβ, and [O III] λ5007) were measured from each individual spectrum. The spectra went deep enough to

[3] The Image Reduction and Analysis Facility (IRAF) is distributed by the National Optical Astronomy Observatories, which are operated by the Association of Universities for Research in Astronomy, Inc., under contract with the National Science Foundation.

TABLE 1
Relative Emission-Line Strengths

Spectral Line	Uncorrected Flux	Corrected Flux
[O II] λ3727	0.033	0.60
[O III] λ4959	0.10	0.35
[O III] λ5007	0.29	0.98
Hβ	0.087	0.35
Hα	1.000	1.00
[N II] λ6584	0.0080	0.0080

detect [O II] λ3727, although this line and the N [II] λ6584 lines were so weak that they could only be measured in the co-added spectrum. Three pertinent regions are shown in Figure 1.

The relative emission-line strengths are given in Table 1. The actual Hα flux measured is only about one-quarter of the total Hα luminosity measured from direct images by MHK03. This is due presumably to slit losses necessitated by remaining at the parallactic angle (position angle $\sim 0^\circ$) that prevented the slit from being aligned with the H II region (position angle $\sim 130^\circ$; see Fig. 3 of MHK03).

2.2. *VLT Observations*

2.2.1. *HIZSS 3 and Reference Field*

Near-IR imaging observations of HIZSS 3 and a nearby reference field were obtained at the ESO VLT during 2003 November. Time for these images was allocated within the ESO Director's Discretionary Time (DDT) program. All VLT observations reported here were executed in Service Mode.

Images were obtained using the short-wavelength (SW) arm of the ISAAC near-IR imaging spectrometer mounted at one of the Nasymth foci of the Antu UT1 8.2 m telescope. The SW arm uses a 1024×1024 Hawaii Rockwell HgCdTe array with a plate scale of 0.148 arcsec pixel^{-1} for a single-image field of view of approximately $2\farcm5 \times 2\farcm5$. ISAAC was operated in its standard jitter mode, in which a series of images is obtained with random telescope offsets of up to $15''$ relative to a fiducial center point between each individual exposure.

A series of such jittered images was obtained for both the HIZSS 3 field ($\alpha = 07^{\rm h}00^{\rm m}26\fs9$, $\delta = -04^\circ 12' 30''$, J2000.0) and a nearby reference field ($\alpha = 07^{\rm h}00^{\rm m}11\fs0$, $\delta = -04^\circ 03' 38''$, J2000.0) using the J_s and K_s filters. The HIZSS 3 field center was chosen to include both the 21 cm peak and the H II region discussed in MHK03 (see that work for coordinates). The reference field was selected to have the identical galactic latitude and contain no very bright stars. It is otherwise unexceptional and located approximately $10'$ away. An additional narrowband Paβ image (ISAAC filter NB_1.28) of the HIZSS 3 field was obtained to allow the determination of foreground reddening. All images were obtained under clear, apparently photometric, conditions (see photometric calibration discussion below). A summary of these observations is provided in Table 2.

The HIZSS 3 and reference field image series were processed by the ESO ISAAC pipeline into single images that were dark-, bias-, and background-corrected. These images were delivered as part of the standard ESO Service Mode data package. Images were processed using the *combine_mc* algorithm, reported to produce photometrically reliable final images.[4] Photometric accuracy was verified by comparing the instrumental magnitudes of stars detected in single frames with the same stars in the combined frames. No systematic trends with respect to position or magnitude were seen within the area in which all images in the series overlapped, confirming the photometric reliability of the pipeline output.

Five output images were delivered: J_s and K_s images for both the HIZSS 3 and reference field pointings, as well as Paβ for the HIZSS 3 pointing. All five output images were trimmed to the same area, corresponding to the output image with the smallest area in which all input images for that stack overlapped. The final size of the trimmed images was 951×951 pixels, corresponding to 19,810 arcsec^2, or 5.503 arcmin^2. The image quality of the output images is excellent: the FWHM of a Gaussian fit to

[4] See http://www.eso.org/projects/aot/eclipse/jitterphot.

TABLE 2
VLT Observation Log

UT Date and Time	Target	Integration (s)	Filter	Air Mass	Seeing (arcsec)
2003 Nov 06 23:40	UKIRT FS29	5×14.2	J_s	1.12	...
2003 Nov 07 00:12	UKIRT FS6	5×14.2	J_s	2.30	...
2003 Nov 07 04:55	UKIRT FS6	5×14.2	J_s	1.18	...
2003 Nov 07 07:00	UKIRT FS112	5×20.0	Paβ	1.09	...
2003 Nov 07 07:11	HIZSS 3	11×180	Paβ	1.11	0.60
2003 Nov 07 07:54	UKIRT FS121	5×20.0	Paβ	1.09	...
2003 Nov 07 08:00	UKIRT FS121	5×20.0	J_s	1.10	...
2003 Nov 07 08:08	HIZSS 3	30×60	J_s	1.11	0.53
2003 Nov 07 23:52	UKIRT FS29	5×14.2	K_s	1.30	...
2003 Nov 08 07:43	HIZSS 3	35×60	K_s	1.07	0.49
2003 Nov 08 09:01	UKIRT FS14	5×14.2	K_s	1.10	...
2003 Nov 08 09:27	UKIRT FS10	5×14.2	K_s	2.28	...
2003 Nov 09 03:50	UKIRT FS6	5×14.2	J_s	1.15	...
2003 Nov 09 04:03	UKIRT FS6	5×14.2	K_s	1.15	...
2003 Nov 09 06:11	Off-field	35×60	K_s	1.21	0.50
2003 Nov 09 07:10	Off-field	30×60	J_s	1.10	0.48
2003 Nov 09 08:57	UKIRT FS14	5×14.2	J_s	1.10	...
2003 Nov 09 09:09	UKIRT FS14	5×14.2	K_s	1.10	...

Notes.—UT time and date indicate the start of the observing sequence. Seeing is reported for final combined images produced by ISAAC pipeline. Seeing is not reported for standard stars.

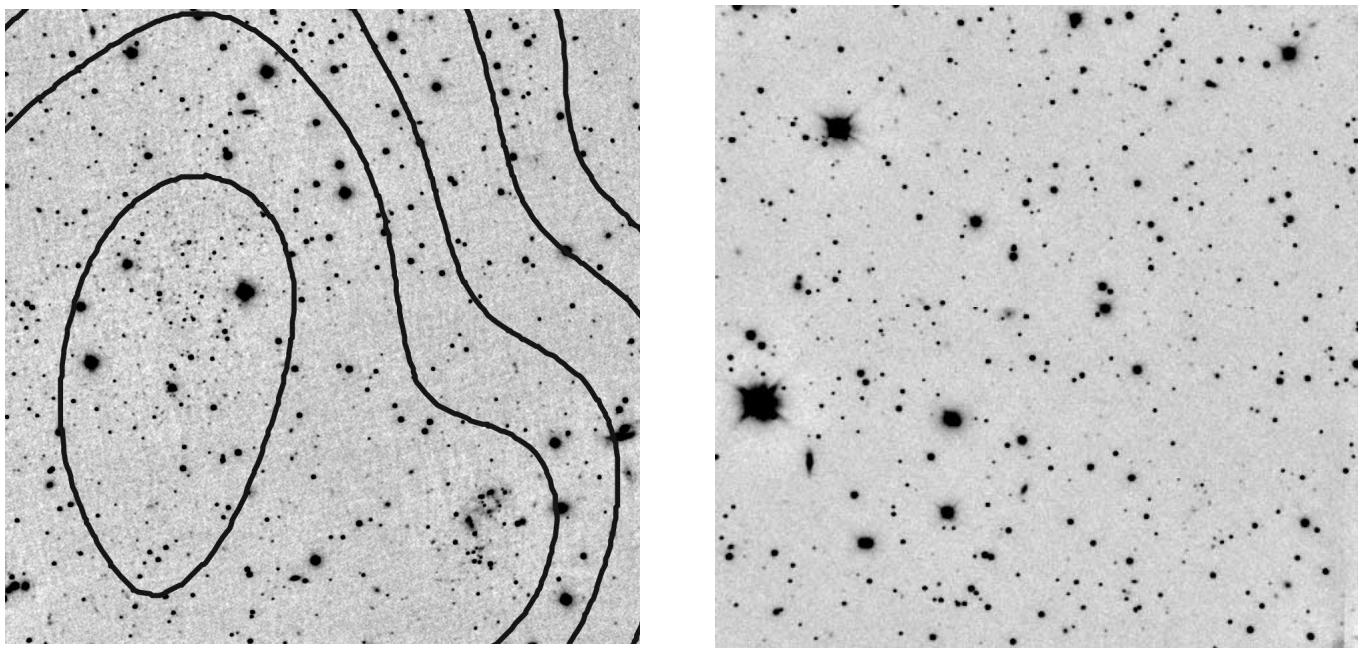

FIG. 2.—K_s HIZSS 3 (*left*) and reference field (*right*) images. North is up, and east is to the left. Each image is $2'.35 \times 2'.35$ in size. In the HIZSS 3 image, the H I contours from MHK03 are overlaid (see their Fig. 1). From inspection, it is clear that there is a faint stellar population associated with the H I peak, while the H II region lies within a bulge in the H I contours. Objects in the reference field are more uniformly distributed and less numerous.

the FWHM is close to $0''.5$ in the J_s and K_s frames and $0''.6$ in the Paβ frame.

These images clearly reveal the stellar content of HIZSS 3 for the first time. The K_s HIZSS 3 and reference field images are shown in Figure 2. The reference field image simply shows a uniform distribution of stars, while the HIZSS 3 field image clearly shows enhanced object surface density at the locations of the H II region and the H I peak. Figure 3 shows zoomed J_s, K_s, and Paβ images of the H II region. This latter figure clearly shows stellar objects associated with the nebular gas.

2.2.2. *Photometric Calibration*

The ESO calibration program provides nightly observations of UKIRT photometric standards (Hawarden et al. 2001) for ISAAC SW imaging observations. Additional observations of red UKIRT standards were obtained in J_s and Paβ on the same nights that the HIZSS 3 Paβ observations were obtained. A summary of the relevant standard stars observations is found in Table 2.

Input images of J and K UKIRT standards for all three nights were processed by the ESO pipeline into standard images that were dark-, bias-, and background-corrected. These output images were delivered as part of the standard ESO Service Mode data package. The Paβ standard images were not processed by the ESO pipeline because the NB_1.28 filter is not supported by the standard pipeline. Therefore, input images were processed manually to correct for bias, dark, and (minimal) background.

The instrumental magnitudes of the J and K UKIRT standards were measured using standard IRAF aperture photometry tools. Apertures of radii 15 pixels ($2''.22$) were used, with sky annulus radii 20 pixels ($2''.96$) and widths 10 pixels ($1''.48$). Each star was observed as a sequence of five observations at different physical locations on the array—essentially, center, upper left, upper right, lower right, and lower left. For each star, the mean and standard deviation was computed from the five individual observations. In all cases, the standard deviation was approximately 0.03 mag. This uncertainty is typical for observations for photometric standards with infrared arrays. It does not arise from photon-counting related statistical reasons but from a combination of uncertainties from flat-fielding and illumination

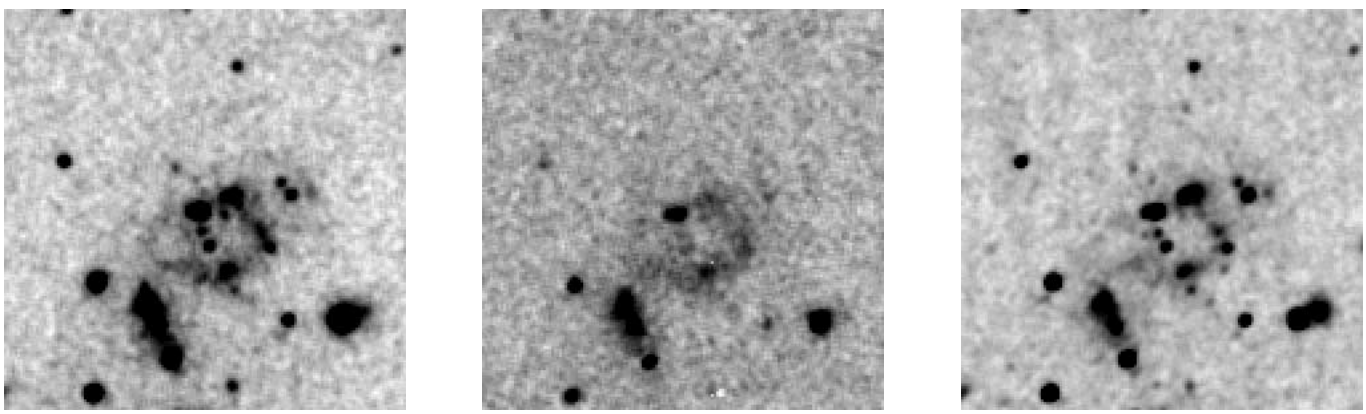

FIG. 3.—Cut-out images of the H II region detected by MHK03. From left to right: J_s, Paβ, and K_s. North is up, and east is to the left. Each image is $22'' \times 22''$.

corrections, light losses from interpixel gaps, bad pixels, and intrapixel sensitivity variations.

Photometric transformation zero points (ζ_i) were computed from each standard star observation using the following equation:

$$\zeta_i = m_i^{\rm cat} - m_i^{\rm ins} - \kappa_i X,$$

where i is the filter, X is the air mass, $m_i^{\rm cat}$ is the catalog magnitude, $m_i^{\rm ins}$ is the mean instrumental magnitude (i.e., the mean of the five individual measurements), and κ_i is the adopted extinction coefficient. Telluric extinction coefficients of -0.07 and -0.05 were chosen for J_s and K_s, respectively, to minimize the scatter between individual zero-point measurements. These values are consistent with the mean values stated in the ISAAC User's Manual. Not enough standard stars were observed to determine reliable color terms independently. However, the ISAAC color terms are thought to be negligible (C. Lidman 2004, private communication).

Final nightly zero points were computed by computing the mean (and standard deviation) of the individual observations. For 2003 November 7 and 9 UT, the J_s zero points are 24.71 ± 0.025 (five stars) and 24.77 ± 0.004 (two stars). For 2003 November 8 and 9 UT, the K_s zero points are 24.16 ± 0.003 (two stars) and 24.14 ± 0.003 (two stars). Combined with the adopted extinction coefficients, these zero points transform instrumental magnitudes into J and K in the UKIRT system (see Hawarden et al. 2001 for transformations to other systems).

The formal uncertainties of the nightly zero points do not provide a definitive constraint on the photometric quality of the relevant nights because of the relatively small number of standard stars observed (see Table 2). What can be said is (1) these measured zero-point values are consistent with the values reported on the ISAAC quality control Web site[5] over a long time period once aperture differences are taken into account, (2) measurements separated by hours on the same night produce zero points consistent to within a few percent, and (3) variations in atmospheric transmission measured by the Paranal ambient site monitor were less than 0.02 mag in the R band during the entire night for all three nights.[6] In conclusion, the nights during which these VLT observations occurred appear to have been photometric at the 0.02 mag or better level.

3. ANALYSIS

3.1. *Foreground Extinction*

Relative emission-line strengths measured in the H II region are given in Table 1. Using the Cardelli et al. (1989) reddening law [$A_{\rm H\beta} = 3.609E(B-V)$ and $A_{\rm H\alpha} = 2.535E(B-V)$] and an intrinsic ratio Hβ/H$\alpha = 0.350$, the derived foreground reddening is $E(B-V) = 1.41 \pm 0.04$, where the error represents the standard deviation of the mean for the eight individual ratios. Using this extinction, corrected flux ratios are given in Table 1. The reddening-corrected line ratio [O III] $\lambda5007/\lambda4959$ is 2.8, in good agreement with the 2.9 value expected on theoretical grounds.

The VLT Paβ images of the H II region can be used to make a similar but independent measurement of the foreground reddening, namely, by comparing the flux of the H II region at Paβ (1.28 μm) to that at Hα. This technique has been recently exploited in a study of spiral galaxies by Jones et al. (2002). The only complication is the lack of spectrophotometric standards in the near-IR, necessitating the use of model atmospheres with *JHK* standards. We are indebted to L. Jones for correspondence and advice on this subject.

The UKIRT standards (Hawarden et al. 2001) FS 112 (G0) and FS 121 (K3) were observed through the ISAAC narrowband 1.28 μm filter (NB_1.28) as well as the broadband J_s and K_s filters. The Kurucz (1992) ATLAS9 $\log g = 4.5$ and $T_{\rm eff} = 6000$ and 4750 K models were adopted for these two stars. For each model, the average fluxes within the J_s and K_s filters were computed. For each star, a conversion factor between model flux (in physical units) and observed flux (in ADUs per second) was computed using the Hawarden et al. (2001) catalog magnitudes, under the assumption that $J_s = 0$ and $K_s = 0$ for Vega. The conversion factors for the two stars agreed within 10%, providing confidence in this procedure.

These conversion factors were then used to transform observed NB_1.28 flux into absolute flux. In order to determine an emission-line flux for a line source, the width of the filter must also be taken into account, i.e., $\int T_\lambda \, d\lambda / T_{1.28\,\mu{\rm m}} = 194$, where T_λ is the transmission of the filter as a function of wavelength.[7] The Paβ count rate was then measured after aligning the J_s image to Paβ and subtracting after matching the PSFs by convolution and scaling. The derived flux at Paβ is 9.88×10^{-15} ergs cm^{-2} s^{-1}. The observed ratio $({\rm Pa}\beta/{\rm H}\alpha = 8.7 \times 10^{-2})_{\rm obs} = 0.45$ (where the flux at Hα has been taken from MHK03) can be compared to the intrinsic ratio $({\rm Pa}\beta/{\rm H}\alpha = 8.7 \times 10^{-2})_{\rm int} = 5.71 \times 10^{-2}$ (Osterbrock 1974). Combined with the Cardelli et al. (1989) reddening law, the foreground reddening was found to be $E(B-V) = 1.32 \pm 0.04$. This is in good agreement with the value found from the MMT optical spectroscopy (1.41 ± 0.04).

The computed mean and standard deviation of these two foreground reddening measurements is $E(B-V) = 1.36 \pm 0.06$. If 1.25 and 2.2 μm are adopted as the effective wavelengths of the J_s and K_s bands, respectively, the Cardelli et al. reddening curve can be used to compute $A(J-K)$: $A_{1.25} = A_J = 0.874E(B-V) = 1.19 \pm 0.06$ mag and $A_{2.2} = A_K = 0.352E(B-V) = 0.48 \pm 0.06$ mag. Therefore, $A_J - A_K = E(J-K) = 0.522E(B-V) = 0.71 \pm 0.06$ mag.

Formally, these foreground extinction measurements are only valid for the line of sight to the H II region. It is quite possible the foreground extinction across the HIZSS 3 field is variable either because of variations in the foreground Galactic dust distribution or (hypothetical) dust within HIZSS 3 itself. For example, the H II region could be more dusty than the rest of HIZSS 3. It is impossible to constrain the magnitude of possible spatially variable foreground reddening without detailed spectrophotometry of the individual stars in HIZSS 3. Thus, a single-valued $E(B-V)$ is adopted for the rest of this paper. As discussed later, this does not have a significant impact on the main conclusions of this work.

3.2. H II *Region Metallicity*

Without detection of the temperature-sensitive [O III] $\lambda4363$ line, quasi-empirical relations between other emission-line ratios and oxygen abundance (the so-called R_{23} method) may be used to approximate the metallicity of the H II region (Pagel et al. 1979). Three approaches are possible:[8]

1. *Classical R_{23} method*.—The R_{23} ratio

$$R_{23} = \frac{[{\rm O\ III}]\ \lambda5007 + [{\rm O\ III}]\ \lambda4959 + [{\rm O\ II}]\ \lambda3727}{{\rm H}\beta} = 5.50$$

[5] See http://www.eso.org/qc.

[6] See http://archive.eso.org/asm/ambient-server. As Start Night, use the UT Date minus 1 day. For Site, select Paranal.

[7] See Jacoby et al. (1987), but beware of an error in eq. (3), in which $F_N(i)$ is used in place of the correct quantity $F_{(i)}$.

[8] We thank D. Hunter for her guidance in this matter.

has been calibrated by Skillman (1989) for the case in which the oxygen abundance is much lower than solar. Using his formula results in a value $\log O/H + 12 = 7.5$.

2. *R_{23} method modified by* [O III]/[N II].—Edmunds & Pagel (1984) use a modified version of the R_{23} method, which relies on using the strength of the N [II] λ6584 line as an additional calibration of R_{23}. The current measurements result in

$$\log \frac{[\text{O III}]\ \lambda 5007 + [\text{O III}]\ \lambda 4959}{[\text{N II}]\ \lambda 6584} = 2.22,$$

yielding a value of $\log O/H + 12 = 7.8$.

3. *R_{23} method modified by* [O III]/[O II].—McGaugh (1991) instead calibrates the R_{23} value with the relative strengths of [O III] and [O II]:

$$\log \frac{[\text{O III}]\ \lambda 5007 + [\text{O III}]\ \lambda 4959}{[\text{O II}]\ \lambda 3727} = 0.35.$$

This yields a value of $\log O/H + 12 = 7.85$.

In summary, $\log O/H + 12 \sim 7.8$, comparable to other metal-poor irregular galaxies in the Local Group, e.g., IC 1613 ($\log O/H + 12 = 7.85$; Talent 1980), WLM ($\log O/H + 12 = 7.77$; Hodge & Miller 1995), and Pegasus ($\log O/H + 12 = 7.93$; Skillman et al. 1997). For comparison, the oxygen abundances of the LMC and SMC are 8.37 and 8.13, respectively (Russell & Dopita 1990), while that of the solar neighborhood is 8.70 (Esteban & Peimbert 1995).

3.3. *Photometric Properties of Resolved Stellar Population*

Stellar objects were identified in the K_s HIZSS 3 and reference field images using the DAOPHOT star-finding routine implemented under IRAF. This routine identifies features that are significantly above the local noise (in this case, 3 σ) and whose roundness and sharpness are typical of stars. After removing objects that fell partially on the edge of the images, 528 objects were detected in the reference field and 739 in the HIZSS 3 field. Although a small percentage of these stellar objects are undoubtedly unresolved background objects at high redshift, we assume henceforth that all the detected objects are stars in the Milky Way or HIZSS 3. As can be seen in Figure 2, the stellar surface density in the HIZSS 3 field is higher near the positions of the H I peak and H II regions reported by MHK03. In the reference field, the stellar surface density is more uniform.

Instrumental aperture magnitudes of the detected stars were measured using IRAF aperture photometry tools. Point-spread function matching was deemed unnecessary given the relatively low stellar surface density (see Fig. 2). Instrumental magnitudes were measured through a 5 pixel (0.″74) radius circular aperture, using background measurements local to each star. Using the same aperture properties and the pixel coordinates of the stars detected on the K_s frames, aperture magnitudes were also measured on the J_s frames after each J_s frame was geometrically aligned with the corresponding K_s frame to subpixel accuracy. A small number of objects in the K_s reference and HIZSS 3 images (3 and 12, respectively) were so faint in the corresponding J_s images that J_s magnitudes could not be measured.

These instrumental magnitudes were transformed to the UKIRT system using the photometric zero points and extinction terms described in the last section. An aperture correction from the 5 pixel radius used for the program stars to the 15 pixel radius used for the standard stars was computed using a few isolated stars in the program fields. This transformation process was repeated independently for all four HIZSS 3 and reference field frames.

The result is a stellar catalog with J and K magnitudes (and corresponding errors) in the UKIRT near-IR photometric system. Note that these magnitudes have *not* been corrected for foreground reddening. In principle, such a correction is possible for stars associated with HIZSS 3 by ignoring possible variations in the foreground dust distribution. As shown below, however, stars can only be assigned to HIZSS 3 on a statistical basis, making a priori extinction corrections of individual magnitudes impossible—a foreground extinction correction can only be made to ensemble properties. It is also impossible to correct foreground stars for extinction because it cannot be assumed that they lie at a common distance; therefore, a simple screen model cannot be assumed.

Using this catalog, the luminosity functions shown in Figure 4 were constructed. Bin widths were set to 0.4 mag to improve statistical significance in each bin. In both panels, the hatched histograms represent the 525 stars with J and K magnitudes in the reference field, and the unhatched histograms represent the 727 stars with J and K magnitudes in the HIZSS 3 field.

Since HIZSS 3 contains only one modest H II region, star formation is clearly not happening throughout the bulk of the galaxy. Thus, the brightest stars in the near-IR should be stars at or near the tip of the first-ascent giant branch (TRGB). In principle, the apparent magnitude and color of the TRGB can be used to constrain distance and metallicity. To detect the TRGB, the methodology of Lee et al. (1993) is adopted. For a range of histogram bin sizes, the HIZSS 3 and reference field K luminosity functions are constructed and then subtracted to produce a background-corrected K luminosity function for HIZSS 3. Each background-subtracted luminosity function is then convolved with a three-element edge detector filter with the values [−2, 0, +2] (i.e., the so-called zero-sum Sobel kernel). The resultant vector has local maxima at the luminosities where histogram discontinuities occur. The center of the *next* luminosity bin is then adopted as the TRGB apparent magnitude. Figure 5 provides illustrative examples for bin sizes of 0.1 and 0.5 mag, corresponding to TRGB edges at $K = 19.80$ and 20.00, respectively.

TRGB edges were determined for bin sizes 0.10, 0.15, 0.20, 0.25, 0.30, 0.35, 0.40, 0.45, and 0.50 mag. For these nine bins, the mean and standard deviation of the TRGB edge brightness is $K = 19.90 \pm 0.09$. This value is consistent with a visual inspection of the luminosity functions shown in Figure 4. After correction for foreground extinction ($A_{2.2} = 0.48 \pm 0.06$; see § 3.1), this value corresponds to $K_0 = 19.42 \pm 0.11$, where the edge brightness uncertainty and the foreground reddening uncertainty have been added in quadrature.

From deeper near-IR observations in the literature, it is known that the object count should continue to increase with magnitude. This is clearly not the case here, as shown in Figure 4. Estimates of the apparent magnitude at which sample incompleteness becomes significant can be made by applying the Sobel edge detection methodology again. For each field and each filter, total luminosity functions (i.e., without background subtraction) were constructed for bin sizes between 0.5 and 0.1 mag using steps of 0.05 mag. Each luminosity function was then convolved with the same three-element edge detection filter as above. For most resultant vectors, significant incompleteness is indicated by the global minimum. The *previous* (i.e., next brighter) bin is adopted as the completeness limit. The mean and standard deviation over all bin sizes are then computed for each field and filter.

The K completeness limits for the HIZSS 3 and reference images were found to be 21.18 ± 0.09 and 21.34 ± 0.21,

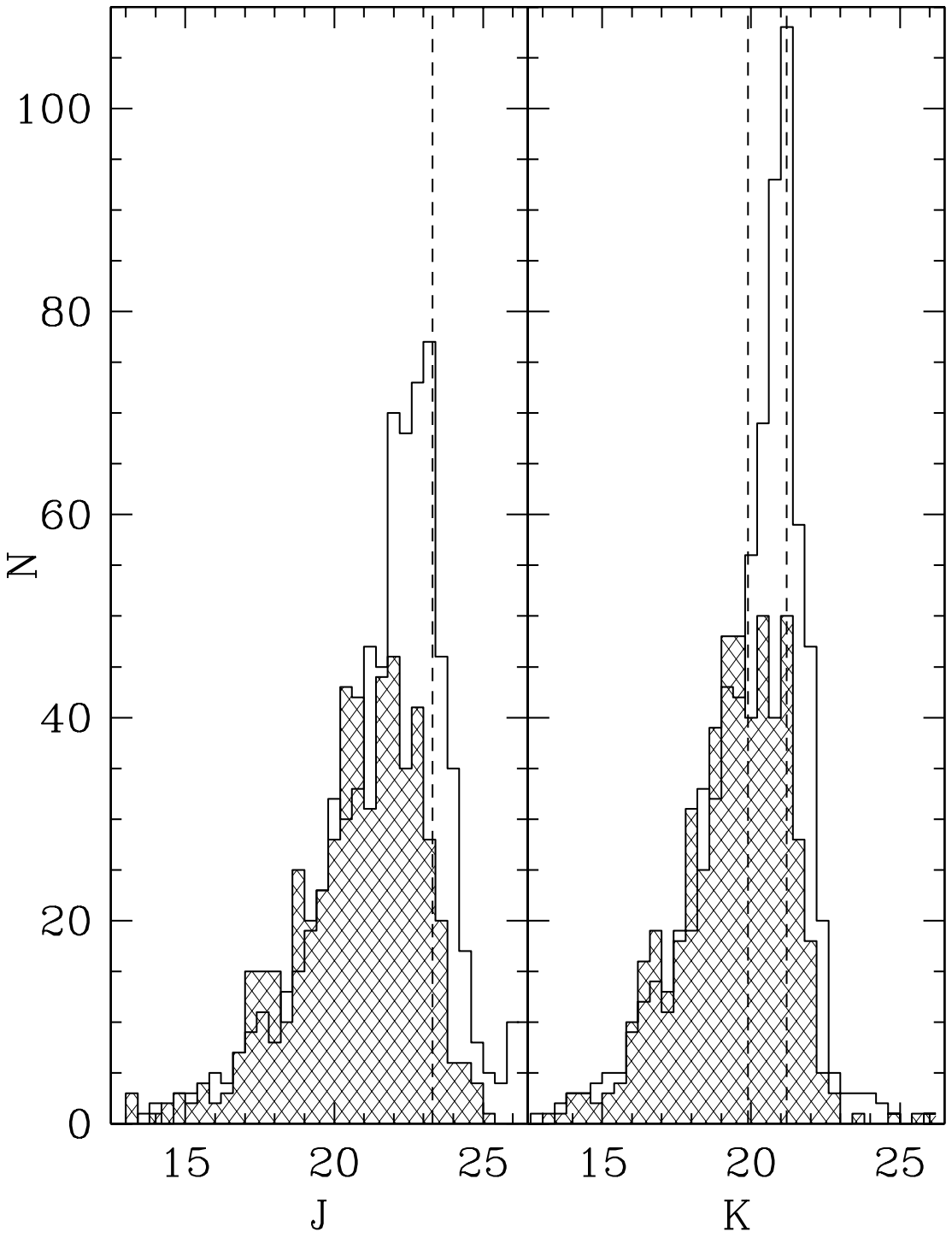

FIG. 4.—*J* and *K* luminosity functions for the stellar objects in the HIZSS 3 and reference field images with *J* and *K* magnitudes. The bin size is 0.4 mag. The hatched luminosity functions contain the 525 stellar objects in the reference field. The nonhatched luminosity functions contain the 727 stellar objects in the HIZSS 3 field. The vertical dashed line in the *J* panel indicates the completeness limit in the HIZSS 3 field. The vertical dashed lines in the *K* panel indicate the adopted TRGB apparent magnitude and the completeness limit in the HIZSS 3 field. [*See the electronic edition of the Journal for a color version of this figure.*]

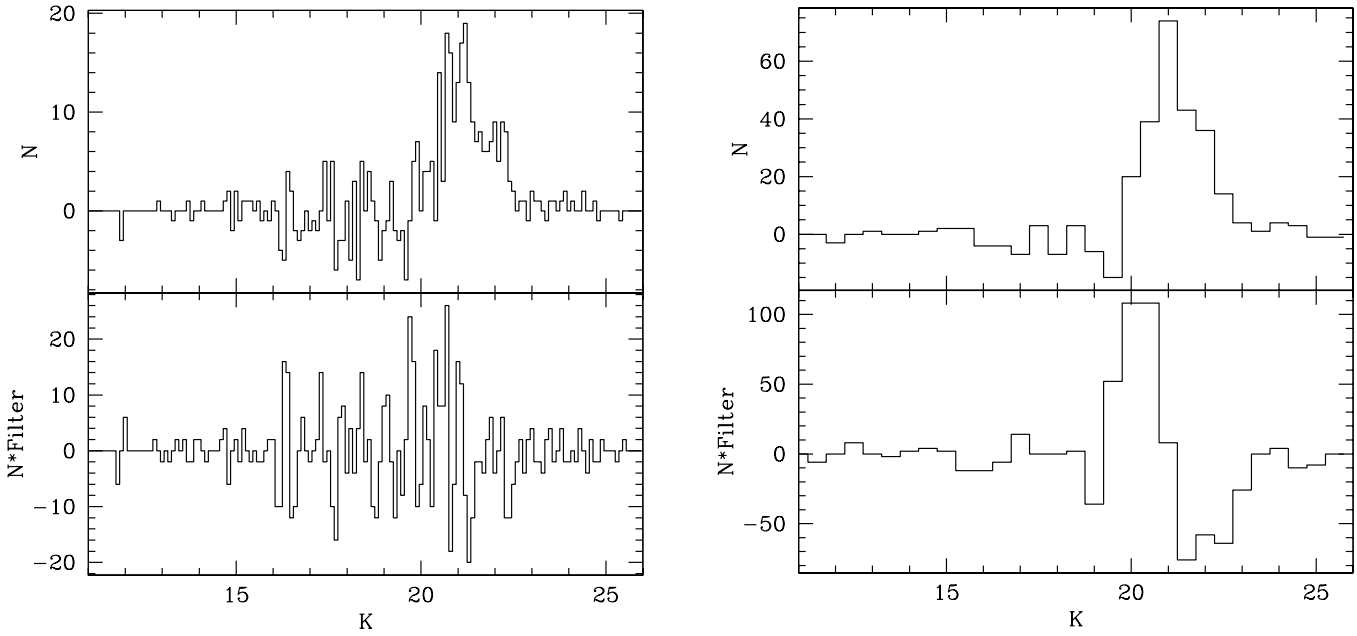

FIG. 5.—Background-corrected *K*-band luminosity function for HIZSS 3 field before (*top panels*) and after (*lower panels*) convolution with Sobel [−2, 0, +2] edge detection filter. Two bin sizes are shown: 0.1 mag (*left*) and 0.5 mag (*right*).

respectively—that is, the same within the errors. The corresponding J completeness limits are 23.33 ± 0.11 and 23.26 ± 0.21—again, the same within the errors. In both filters, the uncertainty of the reference field completeness limit is larger as a result of the detection of fewer sources.

The object catalog constructed above can also be used to construct the HIZSS 3 and reference field CMDs shown in Figure 6. Only objects with $\sigma_{J-K} \leq 0.5$ are shown. In the HIZSS 3 field, there are 44 objects with color uncertainties larger than 0.5 mag, including 12 objects with no measurable J magnitude. In the reference field, the corresponding numbers are 8 and 3.

Looking at Figure 6, it is clear that there are more stars with $J - K \approx 1.9$ in the HIZSS 3 field than in the reference field. This is further quantified in Figure 7, which shows that this excess lies in the approximate color range $1.6 < J - K < 2.2$ for stars with $K > 19.5$ (i.e., slightly above TRGB and fainter) and $\sigma_{JK} \leq 0.2$ mag. For these criteria, there are significantly more objects (141) in the HIZSS 3 field than in the reference field (39). These objects are adopted as red giant branch (RGB) candidates in HIZSS 3. The spatial distribution of these RGB candidates is shown in Figure 8. The RGB candidates are preferentially clumped near the VLA 21 cm H I peak and the H II region, while bluer and redder stars are more uniformly distributed. The median color of the RGB candidates in the HIZSS 3 field is $J - K = 1.87 \pm 0.1$, corresponding to $(J - K)_0 = 1.16 \pm 0.12$ after extinction correction where the color uncertainty has been added in quadrature with the foreground extinction uncertainty. The 13 objects spatially coincident with the H II region emission-line gas are circled in Figure 6. About half (6) of these objects are bluer than the RGB candidates, consistent with them being hotter stars.

3.4. *Stellar Metallicity and Distance Estimates*

Using the extinction-corrected apparent magnitude of the TRGB ($K_0 = 19.42 \pm 0.11$) and adopted median TRGB color ($(J - K)_0 = 1.16 \pm 0.12$), the metallicity and distance to HIZSS 3 can be estimated by comparing the observed HIZSS 3 properties to the properties of Galactic globular clusters as presented by Valenti et al. (2004a, 2004b). These papers are preferred over older papers by the same team (e.g., Ferraro et al. 2000), because all the Galactic globular cluster data have been transformed in a uniform way to the 2MASS photometric system.

Using the UKIRT-2MASS color transformations found on the 2MASS Web site,[9] the adopted median RGB color becomes $J - K_0 = 1.23$ on the 2MASS system. A similar UKIRT-2MASS transformation of K_0 is not necessary given the small (0.003) color term in the published transformation equation. The transformed median TRGB color is consistent with the TRGB colors of the most metal-rich Galactic globular clusters (see Valenti et al. 2004a, Fig. 3), where [Fe/H] lies in the range -0.5 ± 0.1.

Recall that in the H II region, $[\mathrm{O/H}] \sim 7.8\text{–}8.7 = -0.9$; i.e., the nebular gas appears to be significantly more metal-poor than the stars near the TRGB. One speculative explanation for this difference is that the star formation event traced by the H II region is being fueled by gas falling into HIZSS 3 for the first time. In this regard, it should be noted that the H II region lies in a bulge of the H I gas (see MHK03). It is possible that this bulge represents recently arrived gas. Higher spatial resolution velocity maps of the H I gas would be very helpful for investigating this possibility. Such images are currently being obtained and analyzed.

From Valenti et al. (2004b), $M^{\mathrm{TRGB}}_{K_s,\mathrm{2MASS}} \sim -6.7 \pm 0.1$ for metal-rich Galactic globular clusters. Using $K_0 = 19.42 \pm 0.11$ as the foreground extinction-corrected TRGB apparent magnitude (see above), a HIZSS 3 distance modulus of 26.12 ± 0.14 or 1.69 ± 0.07 Mpc is implied. Note that M^{TRGB}_K varies slowly with TRGB metallicity and thus color (see, e.g., Valenti et al. 2004b, Fig. 5). The fact that the adopted TRGB color/metallicity is somewhat uncertain does not have a major impact on the adopted M^{TRGB}_K. Hence, it does not have a major impact on the distance modulus uncertainty. The TRGB-based distance

[9] http://www.astro.caltech.edu/jmc/2mass/v3/transformations.

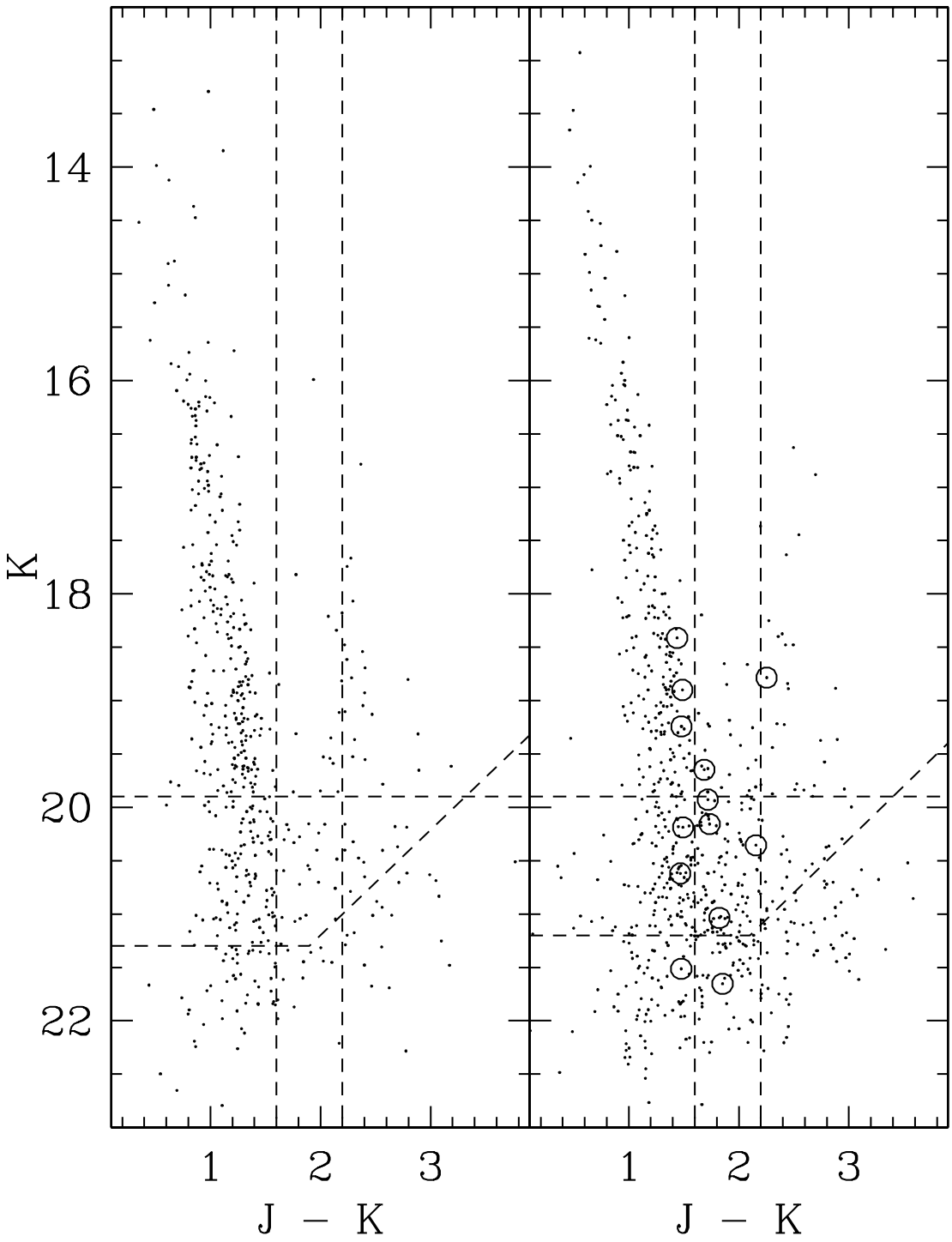

FIG. 6.—CMDs for reference (*left*) and HIZSS 3 (*right*) fields. Only stars with $\sigma_{J-K} \leq 0.5$ mag are shown. The HIZSS 3 TRGB edge at $K = 19.90 \pm 0.09$ is indicated by a horizontal dashed line. The combination of the J and K completeness limits are shown as connected dashed horizontal and diagonal lines. The vertical dashed lines indicate the color region that contains the RGB candidates in the HIZSS 3 field. The circled objects in the HIZSS 3 (*right*) panel indicate stars that are spatially coincident with the H II region emission-line gas. See text for more details.

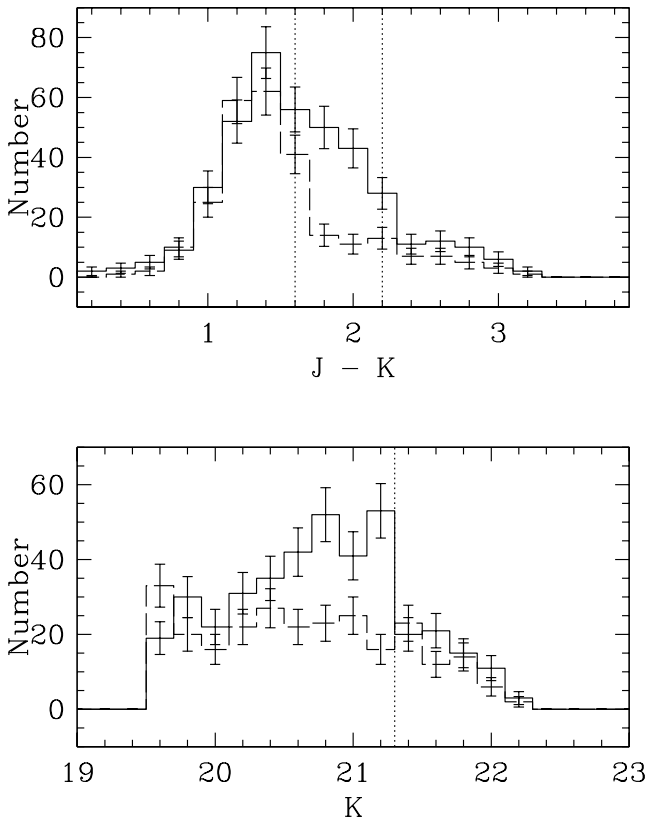

FIG. 7.—Color and luminosity distributions used to select RGB candidates. Only stars with $K > 19.5$ and $\sigma_{J-K} \leq 0.2$ are shown. Neither color nor luminosity are corrected for foreground extinction. In both panels, the solid histogram shows the HIZSS 3 stellar distribution, while the dashed line shows the distribution of objects in the reference field. In the color distribution panel, the vertical dashed lines delineate the color range of the candidate RGB stars in HIZSS 3 (see text). In the luminosity panel, the vertical dashed line shows the adopted K completeness limit. [*See the electronic edition of the Journal for a color version of this figure.*]

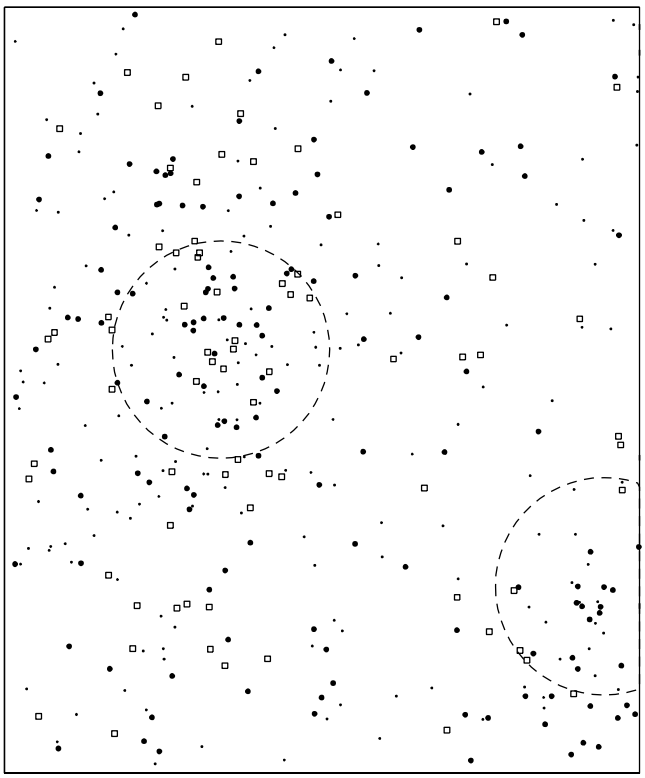

FIG. 8.—Distribution of objects in HIZSS 3 field grouped by color. North is up, east is to the left, and the field of view is $2\farcm35 \times 2\farcm35$ in size (cf. HIZSS 3 K_s image in Fig. 2). Only objects with $K \geq 19.9$ and $\sigma_{J-K} \leq 0.5$ are shown. Small filled circles correspond to $J - K < 1.6$. Large filled circles correspond to $1.6 \leq J - K \leq 2.2$ (i.e., the HIZSS 3 red giant candidates). Open squares correspond to $J - K > 2.2$. The upper dashed circle is centered on the VLA H I peak, while the lower dashed circle is centered on the H II region. Circle centers correspond to coordinates published by MHK03. The circle radii are $20''$. [*See the electronic edition of the Journal for a color version of this figure.*]

estimate is remarkably consistent with the 21 cm redshift estimate of 1.8 Mpc published by MHK03.

Values for the TRGB apparent magnitude and median RGB color have been set from the aggregate properties of stars distributed spatially across the entire HIZSS 3 field. However, a measurement of $E(B - V)$ is only available along one line of sight, i.e., to the H II region contained within HIZSS 3. If this H II region is more dusty than the rest of HIZSS 3, the foreground extinction correction for the TRGB apparent magnitude would be smaller, increasing the estimated distance to HIZSS 3. However, the corrected median RGB color would also become redder, reaching values in excess of median RGB colors of Galactic globular clusters, which seems unlikely. Spatially variable foreground extinction is also possible, but its effects (if present) would be limited to increasing intrinsic $E(B - V)$ uncertainty and thus distance measurement uncertainty. In summary, the adoption of a single-valued $E(B - V)$ does not have a significant impact on the measurement of mean stellar distance or metallicity.

4. CONCLUSIONS

Using data obtained at the MMT Observatory and the ESO Very Large Telescope, the following new properties of HIZSS 3 have been derived:

1. A resolved stellar population has been revealed for the first time. Its near-IR properties are consistent with a TRGB apparent magnitude of $K_0 = 19.42 \pm 0.11$ and a median TRGB color of $(J - K)_0 = 1.22 \pm 0.12$.

2. The line-of-sight extinction to the H II region was found to be $E(B - V) = 1.41 \pm 0.04$ using long-slit spectroscopic observations and $E(B - V) = 1.32 \pm 0.04$ using narrowband Hα and Paβ observations. Given the various uncertainties, this agreement is excellent. The adopted foreground extinction is $E(B - V) = 1.36 \pm 0.06$ for the near-IR photometric measurements.

3. On the basis of emission-line equivalent width measurements, the H II region metallicity was found to be $\log \mathrm{O/H} + 12 \sim 7.8$, corresponding to $[\mathrm{O/H}] \sim -0.9$. In contrast, the mean RGB metallicity was estimated to be $[\mathrm{Fe/H}] = -0.5 \pm 0.1$ using TRGB color. In other words, stars on the RGB appear to be somewhat more metal-rich than the nebular gas. This difference could be explained if the star formation event traced by the H II emission has been fed by lower metallicity gas falling into HIZSS 3 for the first time. Higher spatial resolution maps of the H I gas have been obtained and will be analyzed to investigate this possibility.

4. Using the derived TRGB apparent magnitude of $K_0 = 19.42 \pm 0.11$ and an adopted absolute magnitude of -6.7 ± 0.1, the HIZSS 3 distance modulus was found to be 26.12 ± 0.14, corresponding to a physical distance of 1.69 ± 0.07 Mpc. This estimate is in excellent agreement with distance estimate of $\sim$1.8 Mpc derived from 21 cm redshifts under the assumption of zero peculiar velocity with respect to the Local Group velocity centroid.

These newly derived quantities significantly strengthen the conclusion that HIZSS 3 is a newly discovered dIrr galaxy lurking at the edge of the Local Group. As discussed by MHK03, HIZSS 3 appears to be the nearest dIrr galaxy discovered in the last 25 years. However, the TRGB distance estimate presented here ($\sim$1.7 Mpc) supports the MHK03 conclusion that HIZSS 3 is *not* a member of the Local Group, having more in common with galaxies at a similar distance as Sextans A, Sextans B, NGC 3109, and Antlia.

We thank the ESO Director's Discretionary Time Committee (DDTC) for approving the ESO observations. We also thank Lowell Tacconi-Garman, Emmanuel Jehin, and Wolfgang Hummel for their end-to-end assistance with the VLT observations. We gratefully acknowledge several useful conversations with Deidre Hunter and Lauren Jones. P. M. acknowledges support from NSF grant AST 00-93060. Finally, we thank the anonymous referee for helpful comments and suggestions.

REFERENCES

Cardelli, J. A., Clayton, G. C., & Mathis, J. S. 1989, ApJ, 345, 245
Edmunds, M. G., & Pagel, B. E. J. 1984, MNRAS, 211, 507
Esteban, C., & Peimbert, M. 1995, in Rev. Mex. AA Ser. Conf. 3, Fifth Mexico-Texas Conf. on Astrophysics: Gaseous Nebulae and Star Formation, ed. M. Pena & S. Kurtrz (Mexico: UNAM), 133
Ferraro, F. R., Montegriffo, P., Origlia, L., & Fusi Pecci, F. 2000, AJ, 119, 1282
Hawarden, T. G., Leggett, S. K., Letawsky, M. B., Ballantyne, D. R., & Casali, M. M. 2001, MNRAS, 325, 563
Henning, P. A., Kraan-Korteweg, R. C., Rivers, A. J., Loan, A. J., Lahav, O., & Burton, W. B. 1998, AJ, 115, 584
Henning, P. A., et al. 2000, AJ, 119, 2686
Hodge, P., & Miller, B. W. 1995, ApJ, 451, 176
Jacoby, G. H., Africano, J. L., & Quigley, R. J. 1987, PASP, 99, 672
Jones, L. V., Elston, R. J., & Hunter, D. A. 2002, AJ, 124, 2548
Kurucz, R. L. 1992, in IAU Symp. 149, The Stellar Populations of Galaxies, ed. B. Barbuy & A. Renzini (Dordrecht: Kluwer), 225
Lee, M. G., Freedman, W. L., & Madore, B. F. 1993, ApJ, 417, 553
Massey, P., Henning, P. A., & Kraan-Korteweg, R. C. 2003, AJ, 126, 2362 (MHK03)
McGaugh, S. S. 1991, ApJ, 380, 140
Osterbrock, D. 1974, Astrophysics of Gaseous Nebulae (San Francisco: Freeman)
Pagel, B. E. J., Edmunds, M. G., Blackwell, D. E., Chun, M. S., & Smith, G. 1979, MNRAS, 189, 95
Rivers, A. J. 2000, Ph.D. thesis, Univ. New Mexico
Rivers, A. J., Henning, P. A., & Kraan-Korteweg, R. C. 1999, Publ. Astron. Soc. Australia, 16, 48
Russell, S. C., & Dopita, M. A. 1990, ApJS, 74, 93
Skillman, E. D. 1989, ApJ, 347, 883
Skillman, E. D., Bomans, D. J., & Kobulnicky, H. A. 1997, ApJ, 474, 205
Talent, D. L. 1980, Ph.D. thesis, Rice Univ.
Valenti, E., Ferraro, F. R., & Origlia, L. 2004a, MNRAS, 351, 1204
———. 2004b, MNRAS, 354, 815